Ain Shams Engineering Journal 16 (2025) 103519

Contents lists available at ScienceDirect

Ain Shams Engineering Journal

journal homepage: https://www.sciencedirect.com

Full Length Article

Using treatment and vaccination strategies to investigate transmission dynamics of influenza mathematical model

Zakirullah [a,*], Liang Li [a,*], Kamal Shah [b], Bahaaeldin Abdalla [b], Thabet Abdeljawad [b,c,d,e,*]

[a] School of Mathematical Sciences, University of Electronic Science and Technology of China, Chengdu, 611731, China
[b] Department of Mathematics and Sciences, Prince Sultan University, Riyadh 11586, Saudi Arabia
[c] Department of Mathematics and Applied Mathematics, School of Science and Technology, Sefako Makgatho Health Sciences University, Ga-Rankuwa, South Africa
[d] Department of Medical Research, China Medical University, Taichung 40402, Taiwan
[e] Center for Applied Mathematics and Bioinformatics (CAMB), Gulf University for Science and Technology, Hawally 32093, Kuwait

ARTICLE INFO

Keywords:
Influenza mathematical model
Stability analysis
Sensitivity analysis
Numerical results

ABSTRACT

In this study, we built a deterministic compartmental mathematical model for understanding the transmission dynamics of influenza. The model includes multiple infection phases, including susceptible, exposed, carrier, infected, hospitalized, recovered, and vaccinated populations. Real-world epidemiology data calibrate the model using a least squares optimization approach. The model is mathematically well-posed, with demonstrations of existence, uniqueness, positivity, and boundedness of solutions. The basic reproduction number R_0 is computed using the next generation matrix approach. It is found to be 0.480, showing that a single infected individual, on average, infects less than one person in a completely susceptible population. Stability analysis is performed using a Lyapunov function, revealing that the disease-free equilibrium is locally asymptotically stable when $R_0 < 1$ and globally stable when $R_0 > 1$. Sensitivity analysis suggests that vaccination has a more substantial effect on decreasing transmission compared to treatment. Contour plots of R_0 with respect to key parameters demonstrate that intervention techniques affect epidemic control. Numerical simulations are carried out utilizing the Nonstandard Finite Difference (NSFD) approach to confirm the analytical findings and explore alternative control situations.

1. Introduction

Influenza, commonly referred to as the flu, is a highly infectious respiratory infection caused by influenza viruses, particularly types A and B. The World Health Organization (WHO) estimates that yearly epidemics result in around one billion infections, three to five million severe cases, and two hundred and ninety-five thousand to six hundred fifty thousand respiratory deaths globally. The diseases disproportionately affects vulnerable populations, including the elderly, small children, pregnant women, and individuals with chronic health concerns [2–4]. Clinically, influenza appears with symptoms such as sudden onset of fever, cough, sore throat, muscular pains, fatigue, and headache, whereas many cases are self-limiting, complications might emerge, resulting to pneumonia, worsening of existing conditions, and hospitalization. Influenza has financial impact, including both direct medical expenses and indirect costs from lost productivity. For instance, in the United States, the yearly economic effect of influenza is estimated to be over $11 billion [5].

Vaccination is the most effective technique for avoiding influenza illness and its complications. Seasonal influenza vaccinations are developed yearly to match circulating infectious agents, with effectiveness varied between 40% and 60% depending on the season and population demographics. Despite its demonstrated advantages, vaccination coverage often falls short of the World Health Organization's aim of 75% for high-risk populations. Factors leading to inadequate vaccination rates include vaccine reluctance, limited access to healthcare services, and misinformation. The two primary vaccine types that are most often used are live attenuated influenza vaccines (LAIV) and inactivated influenza vaccines (IIV), which continue to be the cornerstone of influenza prevention. While LAIV, which is provided as a nasal spray, is approved for healthy adults between the ages of 2 and 49, IIV, which is administered by intramuscular injection, is advised for the majority of

* Corresponding authors.
E-mail addresses: zakirullahbzt@gmail.com (Zakirullah), plum.liliang@uestc.edu.cn (Liang Li), kshah@psu.edu.sa (K. Shah), babdallah@psu.edu.sa (B. Abdalla), tabdeljawad@psu.edu.sa (T. Abdeljawad).

https://doi.org/10.1016/j.asej.2025.103519
Received 6 March 2025; Received in revised form 11 May 2025; Accepted 24 May 2025
Available online 30 May 2025

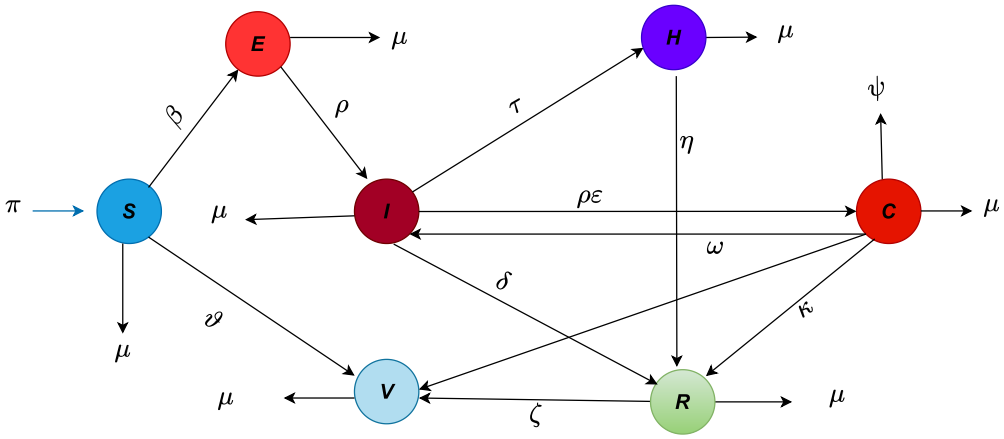

Fig. 1. Compartmental flow diagram illustrating the transmission dynamics of Influenza mathematical model.

age groups, including high-risk populations [6,7]. Recombinant hemagglutinin vaccines (like Flublok) and cell-based vaccinations are recent developments that enhance effectiveness by avoiding egg-adapted mutations. Primary antiviral treatments include neuraminidase inhibitors (oseltamivir, zanamivir) and cap-dependent endonuclease inhibitors (baloxavir marboxil), which, if administered early, reduce the length of symptoms and minimize complications [8]. Subsequently, growing antiviral resistance and variable vaccination efficacy due to antigenic drift underline the need for enhanced universal vaccines and next-generation treatments [9–11].

Mathematical modeling provides a robust framework to evaluate the spreading and progression of infectious diseases within populations via the employing of mathematical equations and analytical methods [12–14]. Mathematical models have been developed in epidemiology to evaluate transmission dynamics and predicted disease behavior [15–18]. Forecasting epidemic outbreaks, assessing the effectiveness of intervention tactics, and assisting public health policy these models. These are also essential instruments for examining disease transmission patterns and forecasting future epidemic trends, offering important information for public health decision-making [19–22]. In order accurately simulate outbreaks, calculate potential infection rates, predict peak incidence periods, and evaluate the potential impact of various control measures, these models incorporate various factors, including demographic variables, disease-specific parameters, and transmission mechanisms. Mathematical modeling plays an important role in guiding public health responses to epidemics, such as decisions concerning vaccination campaigns.

The paper is structured as follows: Section 1 provides an introduction and sets the groundwork for the research. Moving on to Section 2, the model formulation is detailed, encompassing the compartments of the influenza model and their respective parameter descriptions and parameter estimation and data fitting. Section 3 delves into the properties of the SECIRVH model, such as positivity, boundedness and conditions ensuring existence and uniqueness, disease-free equilibrium point, basic reproduction number. Following this, Section 4 investigates the endemic equilibrium alongside local and global stability analyses. Section 5 provides a sensitivity analysis. Section 6 focus shifts to model simulation, which investigates the effects of different input factors on system dynamics. Finally, conclusion is drawn in Section 7.

2. Mathematical model formulation

This section develops epidemiological compartmental models of transmissible diseases for Influenza transmission under hospitalization and vaccination. The total human population N is categorized into six compartments: susceptible S, exposed E, carrier C, infected I, hospitalizated H, recovered R and vaccination V. The parameter π denotes the recruitment or birth rate into the susceptible population. The term β signifies the force of infection, which depends on contact with carriers and can be defined as $\beta = \varpi(I + \chi C)$, where $\varpi = \theta\rho$. Here, θ is the effective contact rate and ρ is a probability of transmission per contact. The value ϑ stands for the vaccination rate of vulnerable people, whereas μ represents the natural death rate. In Fig. 1, the value ε represents the proportion of exposed individuals that develop a mild (carrier) illness. The progression rate from mild infection to severe infection is expressed by ω, while κ reflects the recovery rate from mild illness. The parameter ψ represents the rate at which carriers are screened or removed from the population. The recovery rate from severe infection is provided by δ, and τ reflects the rate at which severe patients are hospitalized. The rate of progression from exposed people to infected ones, corresponding to the inverse of the incubation time, is given by ρ. The parameter η corresponds to the recovery rate of hospitalized individuals, whereas ζ indicates the loss of immunity rate among recovered individuals. Furthermore, χ accounts for the transmission enhancement factor associated with a presence of carriers. In Fig. 1, we present a schematic flow chart of the considered model.

$$
\begin{aligned}
\frac{dS}{dt} &= \pi - (\beta + \vartheta + \mu)S,\\
\frac{dE}{dt} &= \beta S - (\rho + \mu)E,\\
\frac{dC}{dt} &= \rho\varepsilon E - (\omega + \kappa + \mu + \psi)C,\\
\frac{dI}{dt} &= \rho(1-\varepsilon)E + \omega C - (\delta + \tau + \mu)I,\\
\frac{dH}{dt} &= \tau I - (\eta + \mu)H,\\
\frac{dR}{dt} &= \kappa C + \delta I + \eta H - (\zeta + \mu)R\\
\frac{dV}{dt} &= \vartheta S + \zeta R - \mu V,
\end{aligned}
\tag{1}
$$

with the set of initial conditions

$$S(0) > 0,\ E(0) \geq 0,\ C(0) \geq 0,\ I(0) \geq 0,\ H(0) > 0,\ R(0) \geq 0,\ V(0) \geq 0.$$

2.1. Model calibration via least squares optimization

The aim of this section is to estimate the model parameters utilizing actual data from the U.S. epidemic during 2023-2024, with demographic statistics for birth and death rates. The natural birth and death rates were considered constant and estimated based on U.S. census statistics. The daily per capita birth rate π and natural death rate μ were calculated from [1]. The parameter estimate is carried out using the nonlinear least squares approach. The technique starts by establishing an objective function, which is the sum of squared residuals (SSR)

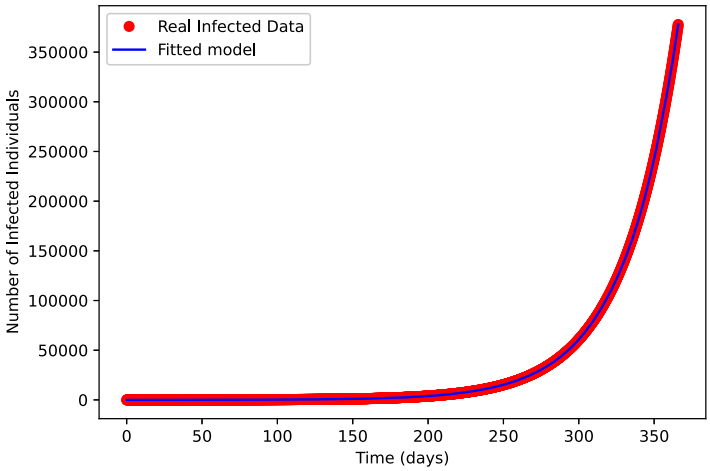

Fig. 2. The model predicted the curve based on the observed data.

Table 1
Fitted model parameters and sensitivity indices.

Parameter	Description	Value	Sensitivity Value	Source
θ	Rate of contact	0.32/day	-	Fitted
μ	Natural death rate	29.55/day	-0.177	[1]
ϖ	Transmission rate	0.020	+1.000	Fitted
β	Force of infection	0.340/day	-0.920	Fitted
χ	Transmission enhancement factor	0.040/day	+0.001	Fitted
κ	Recovery rate from mild infection	0.912/day	-0.201	Fitted
δ	Recovery rate from severe infection	0.010/day	-0.832	Fitted
ψ	Screening or removal rate of carriers	0.023/day	-0.005	Fitted
ρ	Probability of transmission per contact	1.73/day	-	Fitted
ϑ	Vaccination rate of susceptible individuals	0.027/day	-0.073	Fitted
η	Recovery rate from hospitalized individuals	1.9/day	-	Fitted
ρ	Rate of progression from exposed to infectious	0.380/day	+0.005	Fitted
ζ	Loss of immunity rate from recovered individuals	0.095/day	-	Fitted
τ	Rate at which severe cases are hospitalized or treated	0.071/day	-	Fitted
ω	Progression rate from mild infection to severe infection	0.066/day	+0.20	Fitted
ϵ	Proportion of exposed individuals developing mild infection	0.811/day	-0.311	Fitted
π	Recruitment or per capita birth rate into susceptible individuals	0.45/day	+1.000	[1]

that quantifies the difference between model predictions and actual data. Initial parameter values are established based on prior data or estimates, and the model is simulated using these initial values to provide predictions. The SSR is then minimized using the 'lsqcurvefit' optimization approach. A convergence criterion is set, based on the maximum number of repetitions, minimum changes in parameter estimations, or a predefined threshold for the objective function. When the estimated parameters fail to provide a satisfactory match to the actual data or fail to meet the convergence condition, the procedure is restarted by modifying initial values and re-executing the simulation steps until a reasonable agreement is established. This technique guarantees that the model gives a realistic simulation of the epidemic dynamics. The fitted parameter values for the influenza epidemic model are provided in Table 1, whereas Fig. 2 highlights the model of accuracy in replicating observed trends.

3. Model analysis

This section discusses the existence and uniqueness, positivity, boundness, equilibria and basic reproduction number of the model (1)

3.1. Existence and uniqueness

Theorem 3.1. *Given the initial conditions* $S(0) > 0, E(0) \geq 0, C(0) \geq 0, I(0) \geq 0, H(0) > 0, R(0) \geq 0, V(0) \geq 0$, *the system* (1) *exists a unique solution for all* $t \geq 0$ *in the space* $C(R^+, R_+^7)$.

Proof. In vector form, the model system (1) reduces to $\dot{y} = g(y)$

$$\dot{y} = \begin{pmatrix} \dot{S} \\ \dot{E} \\ \dot{C} \\ \dot{I} \\ \dot{H} \\ \dot{R} \\ \dot{V} \end{pmatrix} = \begin{pmatrix} \pi - (\beta + \vartheta + \mu)S, \\ \beta S - (\rho + \mu)E, \\ \rho\varepsilon E - (\omega + \kappa + \mu + \psi)C, \\ \rho(1-\varepsilon)E + \omega C - (\delta + \tau + \mu)I, \\ \tau I - (\eta + \mu)H, \\ \kappa C + \delta I + \eta H - (\zeta + \mu)R \\ \vartheta S + \zeta R - \mu V \end{pmatrix} \tag{2}$$

Each component of the vector field $g(x)$ in system (1) is continuously differentiable almost everywhere in the space

$$C\left(R_+, R_+^7\right),$$

which implies that $g \in C^1$, and hence g is locally Lipschitz continuous.

By the fundamental existence and uniqueness theorem [23], the system of differential equations defined by (1) admits a unique local solution

$$y(t) \in R_+^7, \quad \forall t \geq 0.$$

Since the model describes the dynamics of human population compartments, it is necessary to ensure that all solutions remain nonnegative for all future time $t \geq 0$. This will be established in the following theorem. □

Theorem 3.2. *The region* $\Omega_+ = \{(S,E,C,I,H,R,V); (S(0)>0, E(0)>0, C(0)\geq 0, I(0)\geq 0, H(0)>0, R(0)\geq 0, V(0)\geq 0\}$ *is a positive invariant for model* (1).

Proof. Suppose that (S,E,C,I,H,R,V) is solution of (1), the first equation of the system (1) can be written as follows:

$$\frac{dS}{dt} = \pi - (\beta + \vartheta + \mu)S.$$

This implies,

$$\frac{dS}{dt} \geq -(\beta + \vartheta + \mu)S.$$

By separating variables,

$$\int_{S(0)}^{S(t)} \frac{dS}{S} \geq \int_0^t (\beta + \vartheta + \mu)dt.$$

Thus,

$$S(t) \geq S(0)exp^{-(\beta+\vartheta+\mu)t}, \quad S(0)\geq 0, \forall t > 0. \quad \square \tag{3}$$

Hence the region Ω_+ is a positive invariant and the solution of model (1) will remain inside Ω_+. The remaining equations can be solved with same method: $C(0)\geq 0, E(0)\geq 0, I(0)\geq 0, H(0)\geq 0, R(0)\geq 0, V(0)\geq 0$. Then the solutions $S(t), E(t), C(t), I(t), H(t), R(t), V(t)$ of the model are positive $\forall t > 0$.

3.2. Bounded region for the proposed model

This subsection discusses the boundness of the model (1). Utilize the following theorem to get the bounded feasible region for the proposed model (1).

Theorem 3.3. *The feasible solution set* $\Omega \subseteq R^7$ *of the model* (1) *with initial conditions* $S\geq 0, C(0)\geq 0, E(0)\geq 0, I(0)\geq 0, H(0)\geq 0, R(0)\geq 0, V(0)\geq 0$ *forms a positive invariant set, guaranteeing that all trajectories originating within this set will remain in biologically feasible regions over time.*

Proof. Add all equations of model (1), where

$$N(t) = (S + H + C + I + H + R + V)(t). \tag{4}$$

In the next step, differentiate the equation with respect to time t to obtain

$$\frac{dN}{dt} = \frac{dS}{dt} + \frac{dE}{dt} + \frac{dC}{dt} + \frac{dI}{dt} + \frac{dH}{dt} + \frac{dR}{dt} + \frac{dV}{dt}. \tag{5}$$

Therefore, simplify Eq (5) further yield

$$\frac{dN}{dt} = \pi - \psi C - (I + S + C + R + V + T)\mu,$$

where,

$$S + E + C + I + H + R + V = N,$$

$$\frac{dN}{dt} \leq \pi - N\mu \Longleftrightarrow \frac{dN}{dt} + N\mu \leq \pi. \tag{6}$$

Eq (6) can be calculated using a separable method,

$$\int_{N(0)}^{N(t)} \frac{dN}{\pi - N\mu} \leq \int_0^t dt,$$

This implies,

$$N(t) \leq \frac{\pi}{\mu}(1 - \exp^{-\mu t}) + N(0)\exp^{-\mu t},$$

at $t \to \infty$,

$$N(\infty) \leq \frac{\pi}{\mu}.$$

Hence, solution of the system (1) exists in R_+^7, thus a positive invariant set is constructed as follows:

$$\Omega = (S,C,I,R,V,T) \in R_+^7 : 0 \leq N(t) \leq \frac{\pi}{\mu}. \tag{7}$$

All terms are positive in model (1), so the solution is bounded. $\square$

4. Analysis of the model

This section discusses disease-free equilibrium, reproduction numbers, the local stability of DFE, and its global stability.

4.1. Disease free equilibrium point E_0

When all of the infected components are zero, the E_0 is attained. This condition indicates that there are no infections present in the system (1).

$$\frac{dS}{dt} = \frac{dE}{dt} = \frac{dC}{dt} = \frac{dI}{dt} = \frac{dH}{dt} = \frac{dR}{dt} = \frac{dV}{dt} = 0.$$

Thus, the disease-free equilibrium points for system (1) are expressed as

$$E_0 = \left(\frac{\pi}{\beta + \vartheta + \mu}, 0, 0, 0, 0, 0, \frac{\vartheta\pi}{\mu(\beta + \vartheta + \mu)}\right). \tag{8}$$

4.2. Basic reproduction number (R_0)

R_0 is the average number of infections that the infected person causes over a period of an infectiousness [24].

Theorem 4.1. *The basic reproduction number for model* (1) *is* $R_0 = \frac{\rho\varpi\pi((\omega+\kappa+\mu+\psi)(1-\varepsilon)+\varepsilon\omega+\chi\varepsilon(\delta+\tau+\mu))}{\beta+\vartheta+\mu(\rho+\mu)(\omega+\kappa+\mu+\psi)(\delta+\tau+\mu)}$, *Using the next generation matric.*

Proof. Consider $x = (E,C,I)$, the following system describes the model

$$\frac{dx}{dt} = F(x) - V(x), \tag{9}$$

In this context, $F(x)$ characterizes the generation rate of new infections across the compartments, $V^+(x)$ signifies the influx rate, and $V^+(x)$ denotes the outflow rate.

$$F(x) = \begin{pmatrix} 0 & \varpi\chi S & \varpi S \\ 0 & 0 & 0 \\ 0 & 0 & 0 \end{pmatrix},$$

and the transition matrix as

$$V(x) = \begin{pmatrix} l_1 & 0 & 0 \\ -\rho\varepsilon & l_2 & 0 \\ -\rho(1-\varepsilon) & -\omega & l_3 \end{pmatrix},$$

where,

$$l_1 = \rho + \mu$$

$$l_2 = \omega + \kappa + \mu + \psi$$

$$l_3 = \delta + \tau + \mu$$

The inverse of V is

$$V^{-1} = \begin{pmatrix} \frac{1}{l_1} & 0 & 0 \\ \frac{\rho\varepsilon}{l_1 l_2} & \frac{1}{l_2} & 0 \\ \frac{\rho(l_2+\varepsilon\omega-\varepsilon l_2)}{l_1 l_2 l_3} & \frac{\omega}{l_2 l_3} & \frac{1}{l_3} \end{pmatrix}.$$

The next generation matrix is of the form

$$FV^{-1} = \begin{pmatrix} \frac{S\rho\varpi(l_2+\varepsilon\omega-\varepsilon l_2+\chi\varepsilon l_3)}{l_1 l_2 l_3} & \frac{S\varpi(\omega+\chi l_3)}{l_2 l_3} & \frac{S\varpi}{l_3} \\ 0 & 0 & 0 \\ 0 & 0 & 0 \end{pmatrix}, \tag{10}$$

The eigenvalues of matric (10) are given as

$$\{0, 0, \frac{S\rho\varpi\left(l_2+\varepsilon\omega-\varepsilon l_2+\chi\varepsilon l_3\right)}{l_1 l_2 l_3},$$

Reproduction number R_0 (dominant eigenvalue) is the basic reproduction number.

$$R_0 = \frac{\rho\varpi\pi\left((\omega+\kappa+\mu+\psi)(1-\varepsilon)+\varepsilon\omega+\chi\varepsilon(\delta+\tau+\mu)\right)}{(\beta+\vartheta+\mu)(\rho+\mu)(\omega+\kappa+\mu+\psi)(\delta+\tau+\mu)}. \quad \square$$

4.3. Existence of endemic equilibrium point

In an endemic equilibrium, a disease persists in the population without being eradicated over time. The endemic equilibrium reflects sustained disease transmission, typically occurring when $R_0 > 1$. The endemic point is determined by ensuring that all state variables such as susceptible, exposed, carrier, infected, hospitalizated, recovered and vaccination classes are nonzero at equilibrium $(S^*, E^*, C^*, I^*, H^*, R^*, V^*) \neq (0,0,0,0,0,0,0)$ and by setting the system equations to zero.

Theorem 4.2. *The Eqs. (1) has a unique positive endemic equilibrium point, $E^* = (S^*, E^*, C^*, I^*, H^*, R^*, V^*)$ if and only if the basic reproduction number $R_0 > 1$.*

Proof. If $R_0 > 1$, then the Eqs. (1) possesses a nonnegative endemic equilibrium

$$S^* = \frac{l_2(N-\pi)(\pi-l_1)}{\rho\varepsilon\psi(\vartheta+\mu)}, \tag{11}$$

$$E^* = \frac{l_2(N-\pi)}{\rho\varepsilon\psi}, \tag{12}$$

$$C^* = \frac{l_1(\vartheta+\mu)}{\varpi\chi\left(\pi-l_1\right)} - \mho, \tag{13}$$

$$I^* = \chi\mho, \tag{14}$$

$$H^* = \tau\chi\mho, \tag{15}$$

$$R^* = \mho_1\mho, \tag{16}$$

$$V^* = \zeta\mho_1\mho(R_0-1), \tag{17}$$

where,

$$\mho = \frac{l_2(\rho\varepsilon\omega+1)(\varepsilon-1)(\pi-N)}{\varepsilon\psi\chi(\delta+\mu)},$$

$$\mho_1 = \frac{l_1\kappa(\vartheta+\mu)}{\varpi\chi\left(\pi-l_1\right)(\mu+\zeta)} - \frac{(\kappa+\chi\delta+\chi\tau\eta)}{(\mu+\zeta)}. \quad \square$$

4.4. Stability analysis

This section discusses local and global stability [25].

4.5. Local stability of the disease-free equilibrium (DFE)

Theorem 4.3. *In system (1), the disease-free equilibrium E_0 is local asymptotically stable if $R_0 < 1$, otherwise it is unstable.*

Proof. The Jacobian matrix for the system (1) is given by

$$J = \begin{pmatrix} -(\beta+\vartheta+\mu) & 0 & 0 & 0 & 0 & 0 & 0 \\ \beta & -l_1 & 0 & 0 & 0 & 0 & 0 \\ 0 & \rho\varepsilon & -l_2 & 0 & 0 & 0 & 0 \\ 0 & \rho(1-\varepsilon) & \omega & -l_3 & 0 & 0 & 0 \\ 0 & 0 & 0 & \tau & -(\eta+\mu) & 0 & 0 \\ 0 & 0 & \kappa & \delta & \eta & -(\zeta+\mu) & 0 \\ \vartheta & 0 & 0 & 0 & 0 & \zeta & -\mu \end{pmatrix} \tag{18}$$

Now, at the disease-free equilibrium: $E_0 = (\frac{\pi}{\beta+\vartheta+\mu}, 0, 0, 0, 0, 0, \frac{\vartheta\pi}{\mu(\beta+\vartheta+\mu)})$. The Jacobian matrix at disease-free equilibrium E_0 gives

$$J_{E_0} = \begin{pmatrix} -(\vartheta+\mu) & 0 & 0 & 0 & 0 & 0 & 0 \\ 0 & -l_1 & 0 & 0 & 0 & 0 & 0 \\ 0 & \rho\varepsilon & -l_2 & 0 & 0 & 0 & 0 \\ 0 & \rho(1-\varepsilon) & \omega & -l_3 & 0 & 0 & 0 \\ 0 & 0 & 0 & \tau & -(\eta+\mu) & 0 & 0 \\ 0 & 0 & \kappa & \delta & \eta & -(\zeta+\mu) & 0 \\ \vartheta & 0 & 0 & 0 & 0 & \zeta & -\mu \end{pmatrix} \tag{19}$$

The matrix (19) yields the following eigen values:

$$-\mu, -(\mu+\eta), -(\mu+\zeta), -(\mu+\vartheta), -(\rho+\mu), -(\omega+\kappa+\mu+\psi), -(\delta+\tau+\mu). \tag{20}$$

Local asymptotic stability is achieved for the model because all eigenvalues of Eqs. (20) are real and negative, satisfying the Routh-Hurwitz criterion. $\square$

4.6. Global stability of the disease-free equilibrium

Theorem 4.4. *E_0 of system (1) is globally asymptotically stable inside the invariant set Ω if $R_0 \leq 1$, and unstable otherwise.*

Proof.

$$\begin{aligned} \pounds(S,E,C,I,H,R,T) &= (S-S_0-S_0 In\frac{S}{S_0}) + (V-V_0-V_0 In\frac{V}{V_0}) \\ &\leq (\frac{S-S_0}{S})\frac{dS}{dt} + (\frac{V-V_0}{V})\frac{dV}{dt} \\ &\leq (\frac{S-S_0}{S})(\pi-(\beta+\vartheta+\varphi)S) \\ &\quad + (\frac{V-V_0}{V})(\vartheta S+\zeta R-\varphi V) \\ &\leq -\frac{\pi}{SS_0}(S-S_0)^2 - \frac{\vartheta S_0}{VV_0}(V-V_0)^2. \end{aligned}$$

Thus, $\pounds(S,E,C,I,H,R,T) < 0$ for all $(S,E,C,I,H,R,T) \in \Omega$, if and only if $(S,E,C,I,H,R,T) = (S_0,E_0,C_0,I_0,H_0,R_0,T_0)$, implying that E_0 is the only invariant set where $\pounds = 0$; hence, by the LaSalle invariance principle, E_0 is globally asymptotically stable on Ω. $\square$

4.7. Global stability of endemic equilibrium point

The Lyapunov method determines the global stability of the endemic equilibrium point E_*.

Theorem 4.5. *E_* is globally asymptotically stable inside the invariant set Ω when $R_0 > 1$; otherwise, it becomes unstable.*

Proof. The global stability of the endemic equilibrium point, we apply the Lyapunov function, which is defined as

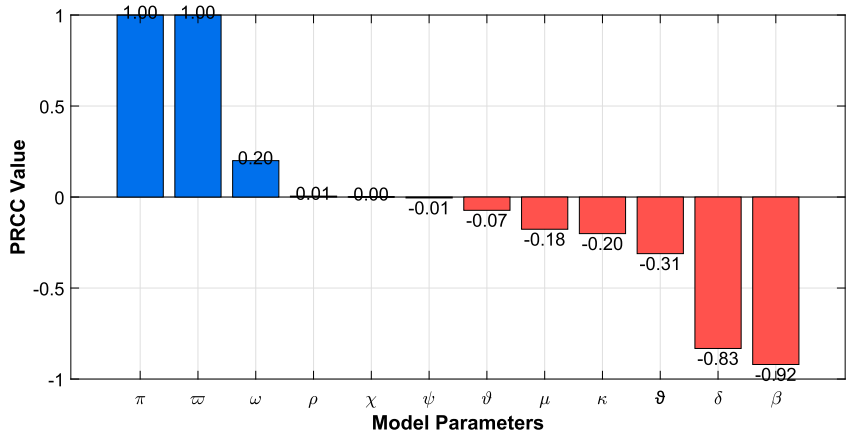

Fig. 3. Compartmental flow diagram illustrating the transmission dynamics of the pneumococcal pneumonia disease mathematical model.

$$
\begin{aligned}
\pounds(S,E,C,I,H,R,T) &= (S-S^*-S^*In\frac{S}{S^*})+(E-E^*-E^*In\frac{E}{E^*})\\
&+(C-C^*-C^*In\frac{C}{C^*})+(I-I^*-I^*In\frac{I}{I^*})\\
&+(H-H^*-H^*In\frac{H}{H^*})+(R-R^*-R^*In\frac{R}{R^*})\\
&+(V-V^*-V^*In\frac{V}{V^*}),\\
\pounds(S,E,C,I,H,R,T) &= (S-S^*)\frac{dS}{dt}+(E-E^*)\frac{dE}{dt}+(C-C^*)\frac{dC}{dt}\\
&+(I-I^*)\frac{dI}{dt}\\
&+(H-H^*)\frac{dH}{dt}+(R-R^*)\frac{dR}{dt}+(V-V^*)\frac{dV}{dt},\\
\pounds(S,E,C,I,H,R,T) &= (\frac{S-S^*}{S})(\pi-(\beta+\vartheta+\mu)S)\\
&+(\frac{E-E^*}{E})(\beta S-(\rho+\mu)E)\\
&+(\frac{C-C^*}{C})(\rho\varepsilon E-(\omega+\kappa+\mu+\psi)C)\\
&+(\frac{I-I^*}{I})(\rho(1-\varepsilon)E+\omega C-(\delta+\tau+\mu)I)\\
&+(\frac{H-H^*}{H})(\tau I-(\eta+\mu)H)\\
&+(\frac{R-R^*}{R})(\kappa C+\delta I+\eta H-(\zeta+\mu)R)\\
&+(\frac{V-V^*}{V})(\vartheta S+\zeta R-\mu V),\\
\pounds(S,E,C,I,H,R,T) &= -\frac{S(S-S^*)^2}{l_1S^*(\vartheta+\varphi)(N-\pi)}-\frac{(E-E^*)^2}{E^*S^*\beta l_2}\\
&-\frac{CI^*(C-C^*)^2}{C^*IS^*(\rho\varepsilon\omega+1)(\varepsilon-1)}\\
&-\frac{C^*E(I-I^*)^2}{I^2C^2E^*l_2^2I\rho\varepsilon\delta\omega(\pi-N)^2}\\
&-\frac{I(H-H^*)^2}{H^*I^*\pi\varepsilon\psi\mathfrak{V}(\varepsilon-1)^2(\delta+\varphi)}\\
&-\frac{\mathfrak{V}(R-R^*)^2}{R^*l_2(\rho\varepsilon\omega+1)\mathfrak{V}_1^2}-\frac{\mathfrak{V}_1\mathfrak{V}(V-V^*)^2}{\zeta V^*}. \quad \square
\end{aligned}
$$

Thus, $\pounds(S,V,E,I,R)<0$ for all $(S,V,E,I,R)\in\Omega$, if and only if $(S,V,E,I,R)=(S^*,V^*,E^*,I^*,R^*)$, implying that E_0 is the only invariant set where $\pounds=0$; hence, by the LaSalle invariance principle, E_0 is globally asymptotically stable on Ω.

5. Sensitivity analysis

The most significant parameters in the model are identified via sensitivity analysis using the concept of an established standard, such as the Partial Rank Correlation Coefficient (PRCC). The sensitivity of R_0 concerning a parameter X is computed as follows:

$$\Gamma_X^{R_0}=\frac{\partial R_0}{\partial X}\times\frac{X}{R_0} \tag{21}$$

$$\Gamma_\pi^{R_0}=1. \tag{22}$$

A sensitivity analysis of the R_0 was performed to determine how model parameter changes affect disease transmission. The sensitivity indices illustrate which factors most significantly affect R_0 positively or negatively. As shown in the Table 1, the recovery rate from severe infection (δ) and force of infection (β) exhibit the highest negative sensitivity indices (-0.832 and -0.920), accordingly suggesting that increases in these parameters significant amounts reduce R_0 and thus have a robust stabilizing effect on the disease dynamics. The progression rate from mild to severe disease (index: +0.02) and the transmission enhancement factor (ω) caused by carriers (index: +0.001), on the other hand, have a positive impact on R_0, indicating that they exacerbate the spread when raised. Additionally, the vaccination rate (ϑ) exhibits a slight negative sensitivity index (-0.073), showing that even minor improvements in vaccination coverage can play a role in decreasing R_0. However, the impact is less dramatic than direct treatment or contact reduction. Parameters such as screening or removal of carriers (ψ) and progression from exposed to infected (ρ) have minimal indices (±0.005, showing limited impact on R_0 under present assumptions. The results from the sensitivity analysis give recommendations for prioritizing control strategies: addressing highly sensitive parameters like contact reduction, boosting treatment rates, and expanding immunization programs can result in the most significant decreases in disease transmission.

6. Numerical results and discussion

This section presents the numerical results for system (1). The Influenza model is simulated using the Nonstandard Finite Difference (NSFD) method with initial conditions set as NSFD method with the initial conditions set as $S(0)=700$, $E(0)=500$, $C(0)=320$, $I(0)=200$, $H(0)=200$, $R(0)=100$, and $V(0)=70$. The parameter values are taken from Table 1. Fig. 3 presents the Partial Rank Correlation Coefficient (PRCC) analysis, which identifies the most influential parameters affecting the basic reproduction number R_0. Fig. 4 depicts a contour plot presenting the basic reproduction number R_0 in the simulation results to four critical parameters: the vaccination rate, the screening or removal rate of carriers, the progression rate from mild to severe infection, and the transmission enhancement factor. Plotting demonstrates that while

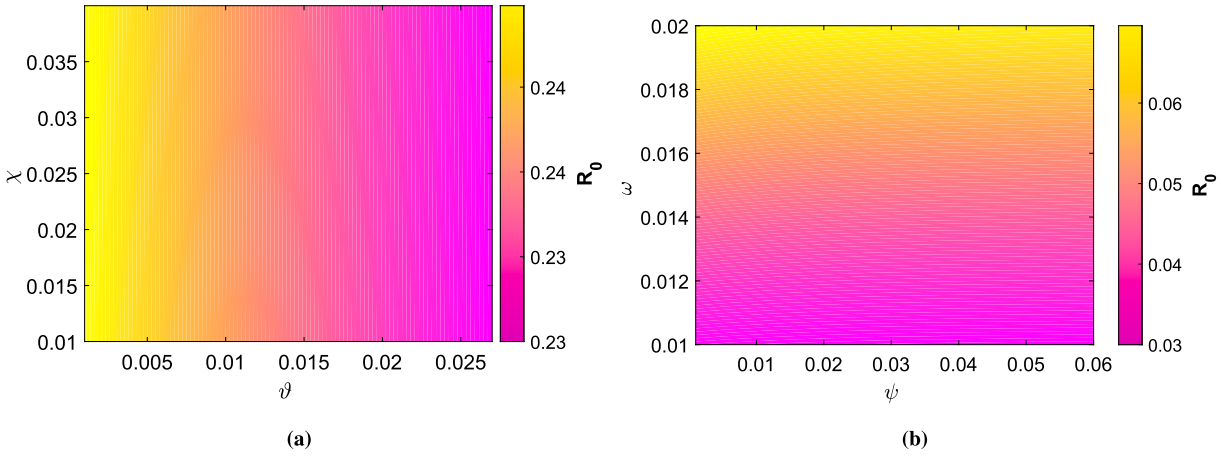

Fig. 4. R_0 vs. Transmission enhancement factor (χ), Vaccinationrate (ϑ), Progression rate from mild infection to severe infection (ω) and Screening/removalrateof-carriers (ψ).

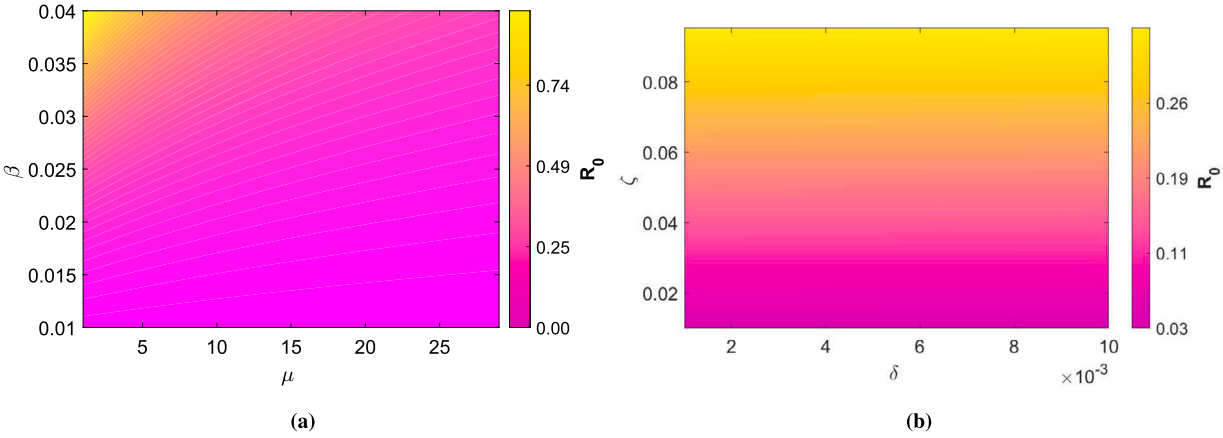

Fig. 5. R_0 vs. Natural death rate (μ), Force of infection (β), Loss of immunity rate from recovered individuals ζ Recovery rate from severe infection (δ).

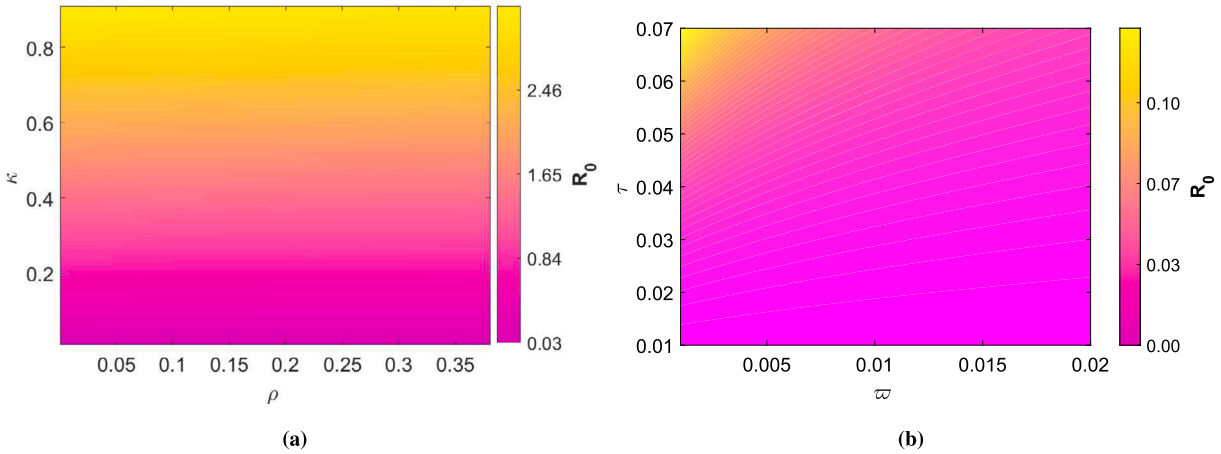

Fig. 6. R_0 vs. Recovery rate from mild infection (κ), Rate of progression from exposed to infectious (ρ), Rate at which severe cases are hospitalized τ and Transmission rate ϖ.

higher transmission enhancement or further progression to severe infection results in increased R_0, showing elevated outbreak risk, improving vaccination and screening rates significantly lowers R_0. The relationship between R_0 and the force of infection, recovery rate from severe illness, loss of immunity from recovered humans, and natural death rate can be seen in Fig. 5. Higher recovery and natural death rates lead to a decrease in R_0, but higher infection force and faster loss of immunity are caused to an increase in R_0, which may result in reinfection and sustained transmission. Also look at the impact of the overall transmission rate, the hospitalization rate of severe cases, the rate of progression from exposing one to an infection, and the recovery rate from mild infections in Fig. 6. As higher progression and transmission rates increase R_0, showing faster disease spread, faster recovery and higher hospitalization rates contribute to lower R_0, suggesting better results through early care

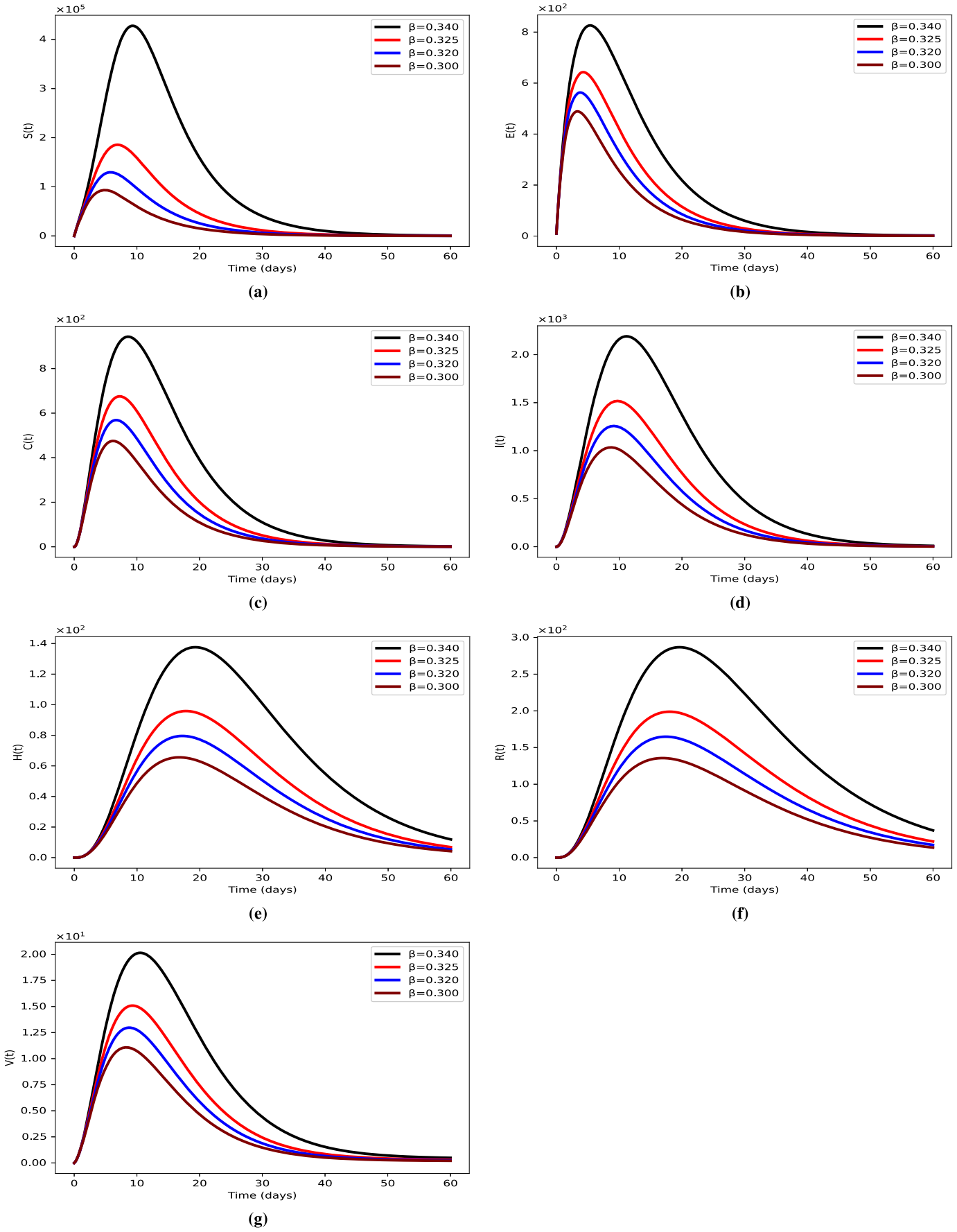

Fig. 7. Profile of Susceptible, Exposed, Carrier, Infected, Hospitalized, Recovered and Vaccinated Populations vs. Force of Infection (β).

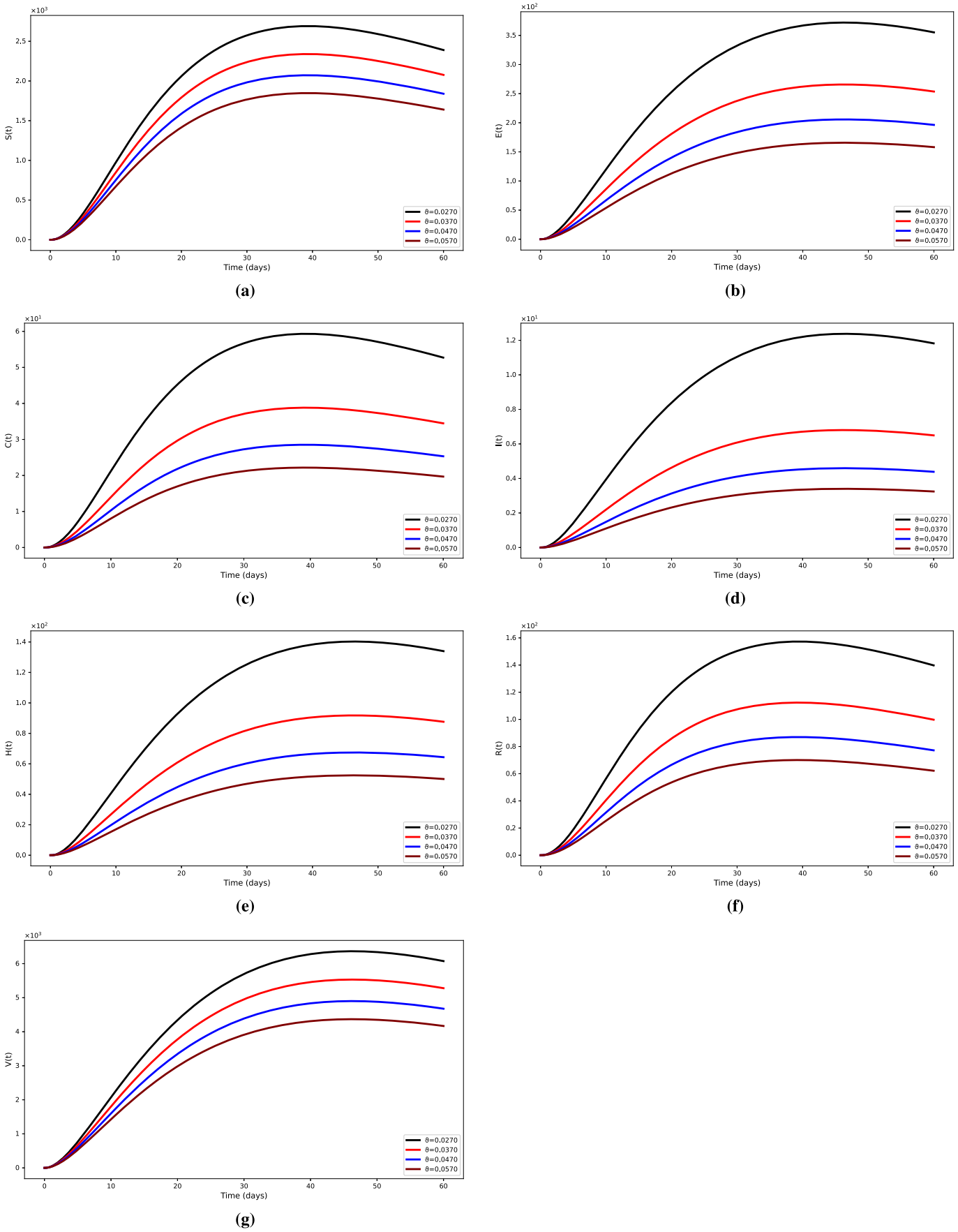

Fig. 8. Profile of Susceptible, Exposed, Carrier, Infected, Hospitalized, Recovered and Vaccinated Populations vs. vaccination rate (θ).

and isolation. It is clear that immunization, screening, and treatment interventions in the early stages are essential for decreasing the R_0. In addition to validating the model of sensitivity analysis, these visualizations offer precise guidance for the parameters that public health policy to give priority in order to effectively control influenza outbreaks.

From Fig. 7, we notice the dynamic impacts of reducing the force of infection β on all compartments of the influenza model. In Fig. 7(a-b), when β declines, the susceptible population (S) increases when the exposed population (E) decreases. This behavior reflects the direct effect of decreased transmission: fewer susceptible individuals become exposed, enabling more to stay uninfected. Fig. 7(c-d) indicates that both the carrier (C) and infected (I) populations diminish dramatically when infection pressure decreases. With fewer exposures, fewer individuals get the mild or severe infection phases, suggesting a reduction of disease progression.

In Fig. 7(e-f), we find a significant decline in the hospitalized population and a slight fall in the recovered population. The dramatic fall in hospitalization stems from fewer severe cases, whereas the decline in recoveries reflects the general drop in infections a fewer people catch the illness, and hence fewer recover. Fig. 7(g) contrasts the susceptible and vaccinated populations, where the susceptible group grows owing to reduced transmission.

Fig. 8(a-g), examine the impact of increasing the vaccination rate ϑ on each class of the influenza model. In Fig. 8 (a-b), when ϑ grows, the susceptible population falls dramatically, as more people are immediately shifted to the vaccinated class. Simultaneously, the exposed population shrinks because fewer susceptible individuals remain at risk of infection. Fig. 8 (c-d) depicts a steady decline in both the carrier and infected classes with increasing vaccination, suggesting that early immunization successfully inhibits transmission and lowers both mild and severe cases.

Fig. 8 (e-f) demonstrates a decrease in the hospitalized population since immunization prevents serious illnesses that would otherwise necessitate hospitalization. The recovered population can decrease or plateau as fewer people recover from the infection. In Fig. 8(g), we show a considerable rise in the vaccinated population accompanying a continuous decrease in the susceptible class, directly illustrating the effect of ϑ in transferring people into a protected condition.

Fig. 8(a-g) follow this pattern by combining additional compartments: in all cases, the infectious-related classes (E, C, I, H) continuously drop with increased vaccination rates, while the vaccinated class develops progressively. In addition to indirectly limiting hospitalizations and community transmission by fostering herd immunity, boosting and lowering the disease burden in both exposed and infected compartments, the results emphasize vaccination as one of the most effective and proactive techniques in reducing influenza epidemics.

7. Conclusion

This paper proposes a comprehensive mathematical model for influenza that integrates real-world data fitting and rigorous analysis of disease dynamics. The model demonstrates that maintaining the fundamental reproduction number below unity is crucial for effective influenza disease control. Analytical and numerical studies demonstrate that raising the vaccination rate significantly reduces the spread of diseases, exceeding treatment-based strategies in reducing transmission. The sensitivity and contour analyses highlight crucial characteristics that impact R_0, driving public health strategies. The NSFD-based simulations further demonstrate the stability and efficacy of vaccination-focused treatments. The model offers a helpful framework for understanding influenza spread and determining control strategies, contributing to more informed and proactive epidemic management. The results conclusively show that vaccination is key for preventing the spread of influenza. The vaccination rate had a substantial effect on decreasing the R_0, out of all the control parameters examined. According to these findings, vaccination strategies can be given top priority when it comes to mitigating epidemics. Future research will concentrate at extending the model and using optimal control theory to optimize control strategies.

CRediT authorship contribution statement

Zakirullah: Formal analysis, Data curation, Conceptualization. **Liang Li:** Investigation, Formal analysis. **Kamal Shah:** Validation, Formal analysis. **Bahaaeldin Abdalla:** Resources, Methodology, Funding acquisition. **Thabet Abdeljawad:** Supervision, Software.

Declaration of competing interest

Does not exist.

Acknowledgement

The authors would like to thank Prince Sultan University for APC and support through Theoretical and Applied Sciences research lab.

Data availability

No data was used in this paper.

References

[1] https://www.cdc.gov/flu/whats-new/flu-summary-2023-2024.html?CDC_AAref_Val=https://www.cdc.gov/flu/spotlights/2023-2024/flu-summary-2023-2024.html?utm_source=chatgpt.com.
[2] World Health Organization. Global influenza strategy 2019-2030. 2019.
[3] Pratt, Ozone D. Influenza and the Causes of Disease.
[4] Tyrrell CS, Allen JLY, Gkrania-Klotsas E. Influenza: epidemiology and hospital management. Medicine 2021;49(12):797–804.
[5] Hanage WP, Schaffner W. Burden of acute respiratory infections caused by influenza virus, respiratory syncytial virus, and SARS-CoV-2 with consideration of older adults: a narrative review. Infect Dis Ther 2024:1–33.
[6] Grohskopf LA. Prevention and control of seasonal influenza with vaccines: recommendations of the advisory committee on immunization practices—United States, 2023–24 influenza season. Morb Mort Wkly Rep, Recomm Rep 2023;72.
[7] Recommendations for prevention and control of influenza in children, 2024–2025: policy statement. Pediatrics 2024;154(4):e2024068507.
[8] Dunkle LM, Izikson R, Patriarca P, Goldenthal KL, Muse D, Callahan J, et al. Efficacy of recombinant influenza vaccine in adults 50 years of age or older. N Engl J Med 2017;376(25):2427–36.
[9] Hayden FG, Sugaya N, Hirotsu N, Lee N, de Jong MD, Hurt AC, et al. Baloxavir marboxil for uncomplicated influenza in adults and adolescents. N Engl J Med 2018;379(10):913–23.
[10] Ikematsu H, Hayden FG, Kawaguchi K, Kinoshita M, de Jong MD, Lee N, et al. Baloxavir marboxil for prophylaxis against influenza in household contacts. N Engl J Med 2020;383(4):309–20.
[11] Erbelding EJ, Post DJ, Stemmy EJ, Roberts PC, Augustine AD, Ferguson S, et al. A universal influenza vaccine: the strategic plan for the national institute of allergy and infectious diseases. J Infect Dis 2018;218(3):347–54.
[12] Rvachev LA, Longini Jr IM. A mathematical model for the global spread of influenza. Math Biosci 1985;75(1):3–22.
[13] Bocharov GA, Romanyukha AA. Mathematical model of antiviral immune response III. Influenza A virus infection. J Theor Biol 1994;167(4):323–60.
[14] Bocharov GA, Romanyukha AA. Mathematical model of antiviral immune response III. Influenza A virus infection. J Theor Biol 1994;167(4):323–60.
[15] Mikolajczyk R, Krumkamp R, Bornemann R, Ahmad A, Schwehm M, Duerr HP. Influenza—insights from mathematical modelling. Dtsch Ärztebl Int 2009;106(47):777.
[16] Anteneh AA, Bazezew YM, Palanisamy S. Mathematical model and analysis on the impact of awareness campaign and asymptomatic human immigrants in the transmission of COVID-19. BioMed Res Int 2022;2022(1):6260262.
[17] Anteneh AA, Bazezew YM, Palanisamy S. Mathematical model and analysis on the impact of awareness campaign and asymptomatic human immigrants in the transmission of COVID-19. BioMed Res Int 2022;2022(1):6260262.
[18] Purohit SD. A novel study of the impact of vaccination on pneumonia via fractional approach. Partial Differ Equ Appl Math 2024;10:100698.
[19] Zanib SA, Ramzan S, Shah MA, Abbas N, Shatanawi W. Comprehensive analysis of mathematical model of HIV/AIDS incorporating Fisher-Folk community. Model Earth Syst Environ 2024;10(5):6323–40.
[20] Ramzan S, Zanib SA, Shah MA, Abbas N, Shatanawi W. Analytical study of a modified monkeypox virus model using Caputo–Fabrizio fractional derivatives. Model Earth Syst Environ 2024;10(5):6475–92.

[21] Lu C, Li L, Shah K, Abdalla B, Abdeljawad T. Mathematical insights into chaos in fractional-order fishery model. Model Earth Syst Environ 2025;11(3):1–17.
[22] Ramzan S, Zanib SA, Shah MA, Abbas N, Shatanawi W. On bifurcation analysis and numerical investigation of alcohol consumption dynamics. Mod Phys Lett B 2024;2550040.
[23] Perko L. Differential equations and dynamical systems (vol. 7). Springer Science & Business Media; 2013.
[24] Van den Driessche P, Watmough J. Reproduction numbers and sub-threshold endemic equilibria for compartmental models of disease transmission. Math Biosci 2002;180(1–2):29–48.
[25] Korobeinikov A, Wake GC. Lyapunov functions and global stability for SIR, SIRS, and SIS epidemiological models. Appl Math Lett 2002;15(8):955–60.

Zakirullah: PhD Scholar in University of Electronic Science and Technology of China, Chengdu, China. His research interest is related to mathematical biology.

Prof. Liang Li: Professor of Mathematics in University of Electronic Science and Technology of China, Chengdu, China. His research interest is related to applied mathematics.

Dr. Kamal Shah: Associate Professor and senior researcher in the Department of Mathematics and Sciences, Prince Sultan University Riyadh Saudi Arabia. His area of research is devoted to fractional calculus, mathematical modeling and simulations.

Dr. Bahaaeldin Abdalla: Associate in mathematics and Sciences, Prince Sultan University Riyadh Saudi Arabia. His area of research devoted to differential geometry and calculus.

Prof. Thabet Abdeljawad: Professor in mathematics and Sciences, Prince Sultan University Riyadh Saudi Arabia. His research interested is related to applied analysis and fractional calculus.